Kavitha M., et al. *Nanosystems: Phys. Chem. Math.*, 2025, **16** (5), 669–680. http://nanojournal.ifmo.ru **DOI 10.17586/2220-8054-2025-16-5-669-680** 

# Incorporating manganese selenide with polymerized reduced carbon sheets: an efficient and stable electro-catalyst for methanol oxidation

Kavitha Murugan<sup>1,a</sup>, Kalaiarasi Senthurpandi<sup>2,b</sup>, Vedhi Chinnapaiyan<sup>1</sup>, Muthuchudarkodi Rajaram<sup>1</sup>

<sup>1</sup>PG and Research Department of Chemistry, V.O. Chidambaram College, Thoothukudi-628008, Tamilnadu. Affiliated to Manonmaniam Sundaranar University, Abishekapatti, Tirunelveli-627012, Tamilnadu, India <sup>2</sup>PG and Research Department of Chemistry, A.P.C Mahalaxmi College for Women, Thoothukudi-628002, Tamilnadu, India

<sup>a</sup>kavithakrithiv35@gmail.com, <sup>b</sup>kalaiarasi@apcmcollege.ac.in

Corresponding author: Kavitha Murugan, kavithakrithiv35@gmail.com

ABSTRACT Reduced graphene oxide/Manganese selenide @Poly-N-methyl pyrrole (RGO/MnSe@P-NMPy) polymer nanocomposite are synthesized via chemical oxidative in-situ polymerization process. The RGO/MnSe@P-NMPy polymer nanocomposite was examined using FTIR spectroscopy, UV-Visible, XRD, TEM and electrochemical investigations in addition to FESEM with EDAX. The methanol oxidation reaction in basic environments was validated using the cyclic voltammetry method. The RGO/MnSe@P-NMPy polymer nanocomposite electro-catalyst shows excellent electrocatalytic activity, lower oxidation potential (0.1 V), improved current density (96 mA/cm²), and excellent stability towards methanol oxidation reaction (MOR) in basic medium. It was observed RGO/MnSe@P-NMPy nanohybrid electrocatalyst, the ECSA value is 183.7 m²/g. This result clearly depicts that RGO/MnSe@P-NMPy polymer nanocomposite electro-catalyst has more active sites for MOR reaction. Chronoamperometry was utilized to show that, in comparison to the other nanocomposite, the existence of RMP polymer nanocomposite enhanced stability (1000's) and produced higher current densities (27.71 mA/cm²) for methanol oxidation. According to the results, the P-NMPy introduction in RGO/MnSe structure can enhance the performance of methanol oxidation and increase the resistance to CO in comparison with mono metallic catalyst. This study makes the case for the potential development of high-performance, inexpensive catalysts for energy storage, conversion and useful uses.

KEYWORDS RGO, MnSe, Poly-N-methyl pyrrole (P-NMPy), RGO/MnSe@P-NMPy (RMP), current density, methanol oxidation reaction (MOR)

ACKNOWLEDGEMENTS The authors are extremely grateful to Department of Science and Technology (FAST TRACK and FIST) New Delhi, INDIA for using CHI Electrochemical workstation at V.O. Chidambaram College, Tuticorin-8 and Jasco UV-VISIBLE Spectrophotometer. We are thankful to The Secretary of A.P.C Mahalaxmi College for women, Thoothukudi.

FOR CITATION Kavitha M., Kalaiarasi S., Vedhi C., Muthuchudarkodi R.R. Incorporating manganese selenide with polymerized reduced carbon sheets: an efficient and stable electro-catalyst for methanol oxidation. *Nanosystems: Phys. Chem. Math.*, 2025, **16** (5), 669–680.

#### 1. Introduction

Graphene oxide layers undergo reduction to eliminate oxygen functional components, which increases the material's electrical conductivity, this results in RGO. For the effective reduction of GO, reducing agents such sodium borohydride, hydroquinone, hydrogen sulphide, and hydrazine hydrate have been utilised extensively [1]. There has been a lot of interest in the optical, electrical power and transport properties of transition metal dichalcogenides and chalcogenides [2]. One of the carbon-based materials that have been extensively studied is oxide of reduced graphene (RGO), due to its exceptionally large surface area, chemical stability, and excellent electrical conductivity. Transition-metal chalcogenides MXn (where X is one of S, Se, or Te and M is a transition metal) generated a lot of fascination owing to their unique optical, magnetic, and electrical characteristics [3–5]. For modifying the characteristics and improving the performance of nanocrystals (NCs) in a wide range of applications, such as solar cells [6], electro-catalysts, spintronic devices, and biological labelling, it has always been thought that control over the NCs' size and shape is essential. Therefore, research into the production and manipulation of MnSe<sub>2</sub> at the nanoscale has garnered a great deal of interest [7, 8]. One crucial component of the first row of transition metals is manganese. Manganese compounds are valuable electrode materials due to their inexpensive cost, high operating voltage, good natural abundance, and environmental friendliness. Recent years have seen research on manganese selenide for magneto optical devices, super capacitive behavior, battery applications

and thermoelectric properties [9]. The electrochemical performance should therefore be enhanced by attaching MnSe on RGO

There are two main approaches to enhance catalysts: either by making electro-catalysts more intrinsically active or by enhancing the amount of active sites on the electrode surface [10]. The catalytic activity of MOR may be substantially enhanced by the combined action of Ni and WC species. Incorporating hetero atoms is an effective method for enhancing the intrinsic activity of catalysts [11]. The microstructure engineering of the electrical and crystal structures can be changed by doping foreign materials into the bulk catalysts [12]. The adsorption and desorption capabilities of the reaction intermediates would change as a result of the dislocations in the initial lattice and the local electron redistribution caused by the heteroatoms' distinct atomic radii, thus altering the catalytic performance [11, 13]. One process that has been extensively studied for creating hydrogen from alcohols (methanol) is methanol electro-oxidation into hydrogen and carbon dioxide.

Numerous compounds based on carbon have been found that enhance the cost-effectiveness and catalytic activity of methanol oxidation [14]. Generally speaking, the anode catalyst has strong stability, high toxin tolerance, and high electro-catalytic activity, all of which greatly contribute to the high MOR efficiency. Recent research has categorized exceptional electro-catalysts as nanoparticles possessing a high specific surface area, excellent electrical conductivity, and remarkable durability even under severe electrochemical conditions [15–17]. In addition the enhanced polarization of the MnSe interface, RGO/MnSe interface and P-NMPy/MnSe interface can possibly be the source of the EA enhancement seen in our work. As far as we are aware, no prior research on the RGO/MnSe@P-NMPypolymer nanocomposite has been published. In this work, a straightforward chemical oxidative polymerization technique has been used to successfully manufacture the triple-component nanocatalyst, RGO/MnSe@P-NMPy. When all three components are incorporated together, new electrode materials with dramatically better electrochemical features are produced. Furthermore, increasing the active surface area and electrical conductivity of catalysts is required to enhance their performance. When compared to P-NMPy/MnSe, RGO/MnSe and MnSe electro-catalysts, the RGO/MnSe@P-NMPy nanohybrids significantly outperform them in alkaline media for the methanol oxidation reaction (MOR), exhibiting greater reactivity and stability.

## 2. Experimental section

#### 2.1. Materials and nethods

- 2.1.1. Synthesis of MnSe nanoparticles. In a beaker, ethylene glycol, hydrazine hydrate, and double-distilled water were combined in a 3:1:7 ratios. Using a magnetic stirrer, the mixture was stirred for thirty minutes. One gram of MnCO<sub>3</sub> salt was added, and the mixture was agitated for a further thirty minutes to aid in dissolving. The mixture was then refluxed for three hours at 90  $^{\circ}$ C after 0.5 g of Na<sub>2</sub>SeO<sub>3</sub> powder was added. The mixture was vacuum-filtered and then rinsed with ethanol and double-distilled water when a black precipitate formed. The resultant dark residue was then vacuum-dried for 20 minutes and heated in a hot air oven at 60  $^{\circ}$ C for six hours.
- 2.1.2. Synthesis of P-NMPy decorated MnSe binary nanocomposite. For this process, synthetic MnSe was employed. 0.1 g of MnSe was dispersed 30 ml of water with sonicated at 30 mins. 2.48 g of (0.1 M) FeCl<sub>3</sub> was dissolved in 30 ml of (0.1 M)HCl with magnetic stirring for one hour. Then (0.1 M) of N-Methyl Pyrrole was dissolved in 30 ml of HCl(0.1 M) and stirred under an ice bath for one hour. Following an hour, the solutions of FeCl<sub>3</sub> and MnSe were combined with the monomer solution under an ice bath. The mixture was continuously stirred for 6 hours. After 6 hours, the reaction mixture was left undisturbed for an additional 12 hours, during which a black-colored residue formed. The black residue was filtered, and distilled water was used to wash the residue to remove any impurities. To further purify the final product, it was treated with an appropriate amount of ethanol and then dried in a vacuum oven at 60 °C.
- 2.1.3. Synthesis of RGO decorated MnSe nanocomposite. 0.02 g of synthesized RGO was ultrasonicated at 30 min. At room temperature, ethylene glycol, hydrazine hydrate, and double-distilled water were combined in a 3:1:7 ratio while being stirred magnetically. Followed by addition of 0.83 g of MnCO<sub>3</sub> salt and 1.12 g of Na<sub>2</sub>SeO<sub>3</sub> were dissolved in 70 ml deionised water under vigorous magnetic stirring for 30 min to facilitate the dissolution. Dirty color solutions appeared immediately and get well dispersed status, and then the mixture was transferred into the round bottom flask. The RGO solution was added to the above mixture, and then kept under 90 °C mantle at 3 h. Following filtration, the precipitate was rinsed with an appropriate volume of ethanol to further purify it. Subsequently, the purified precipitate was dried in a vacuum oven at 60 °C.
- 2.1.4. Synthesis of RGO/MnSe@P-NMPy ternary polymer nanocomposite. The synthesized RGO/MnSe was used for this reaction.0.1 g of RGO/MnSe was dissolved 30 ml of water with sonicated at 30 mins. 2.48 g (0.1 M) of FeCl<sub>3</sub> was dissolved in 30 ml of (0.1 M) HCl with magnetic stirring for one hour. Then (0.1 M) N-Methyl Pyrrole was dissolved in 30 ml of HCl (0.1 M). This mixture was stirred under ice bath for one hour. After one hour the FeCl<sub>3</sub> solution and monomer solution was combined with the RGO/MnSe solution. The combined solution was continuously stirred under an ice bath for 6 hours. After completing the reaction, the resulting mixture was permitted to entirely polymerize for 12 hours, and the residue was vacuum-filtered out. Double-distilled water and ethanol were used to wash the precipitate.

After washing, the precipitate was air dried for 20 minutes. Finally, the precipitate was heated in a hot air oven at 60 °C for 6 hours to complete the drying and purification process.

#### 2.2. Characterization

Computer controlled Thermo Scientific Instrument with iD Transmission (Model P4600) was used to record the FTIR spectra, which was then followed by the KBr pellet method. Photoluminescence (PL) Spectra of the samples were recorded on a spectrofluorometer (JASCO, FP8300). The computer controlled XRD system JEOL IDX 8030 was used to record the X-ray diffraction of samples. EDAX and FESEM measurements were carried by JEOL JSM-6700F field emission scanning electron microscope. The atomic force microscopy was completed with Nanosurf easy2scan B02218 profilemeter; a sharp cantilever tip interacts with the sample surface sensing the local forces with the molecules and tip. TEM (High Resolution with EDX). FEI-TECHANAI T20. The electrochemical behaviors of nanocomposite have been investigated through CH-Instrument INC., TX, USA.

#### 3. Results and discussion

## 3.1. Spectroscopic studies

Using UV-visible spectroscopy, the development of the RGO/MnSe@P-NMPy nanocomposite has been investigated. The absorbance was measured between 200 to 800 nm. The  $\pi$ - $\pi$ \* transition may be connected to the peak in the MnSe at 285 nm shown in Fig. 1(a). As can be seen, the UV-Vis absorption spectra of P-NMPy using MnSe nanocomposite material. The figure unequivocally demonstrates that the three prominent peaks in both absorption spectra located at 293, 361 and 566 nm are caused by the  $\pi$ - $\pi$ \* and n- $\pi$ \* transitions. Compared to pure MnSe, there is a larger wavelength shift at 293 nm when MnSe nanoparticles are introduced to P-NMPy chains. The transitions involving the highest occupied molecular orbital (HOMO) and the lowest unoccupied molecular orbital (LUMO) in conducting polymers are generally denoted as  $\pi$ \* and  $\pi$ , respectively [18]. The absorption peaks at 361 and 566 nm correspond to the polaron- $\pi$ \* transitions observed in P-NMPy and MnSe/P-NMPy structures, respectively [19]. The production of RGO/MnSe hybrid nanomaterial is depicted in figure. It is noted that absorbance bands, characteristic of RGO and MnSe surface plasmon resonance band, occur at 302 nm, suggesting the formation of MnSe nanoparticle of the RGO [20,21]. Due to the oxidised condition of P-NMPy, two tiny absorption peak in the 470 – 598 nm regions are responsible to the bipolaron transition [22]. P-NMPy was identified to lead to a red shift in the absorption band, which indicated a reduction in the electronic transition's band gap.

The FT-IR spectra of MnSe, P-NMPy/MnSe, RGO/MnSe and RMP nanocomposite, which were acquired from the materials, are displayed in Fig. 1(b). FTIR spectroscopy was employed to analyze the functional groups found in the generated samples across the spectral range from 4000 to 500 cm<sup>-1</sup>. The vibrations of Mn–Se have been attributed to the high frequency modes at 604 and 529 cm<sup>-1</sup> [23]. When the concentration of the inorganic filler (MnSe) rose, the band found that the band at 2924 and 2362 cm<sup>-1</sup> for MnSe were significant. Owing to the water molecules adhered to the materials layer, the large absorption at 3422 cm<sup>-1</sup> is attributed to the O–H stretching vibration mode. The P-NMPy/MnSe spectrum was illustrating the absorption frequencies, which support the creation of P-NMPy as a result of the identified distinctive peaks. The broad peak in the P-NMPy spectra at 3421 cm<sup>-1</sup> is caused by the N-H stretching vibration. The band at 1638 cm<sup>-1</sup> was found to be C=C and C-C stretching of the P-NMPy rings. For C-N and C-C, band at 1448 cm<sup>-1</sup> was attributed to P-NMPy ring stretching vibration, while the peak at 1384 cm<sup>-1</sup> was assigned to plane distortion. The peak 1050 cm<sup>-1</sup> was associated with the distorted vibrations of C-H and C-N [24]. Two vibration peaks at 1161 and 880 cm<sup>-1</sup> were identified as the stretching peaks of P-NMPy, and the polymerization of pyrrole was suggested by the =C-H out of plane vibration [23, 25]. The existence of the band at 772 cm<sup>-1</sup> indicated the presence of polymerized pyrrole [23]. Because of the significant interaction between P-NMPy and MnSe, the P-NMPyat 1161 and 1050 cm<sup>-1</sup> shift to lower wave numbers. Lower wave numbers are shifted by the P-NMPy at 1161 and 1050 cm<sup>-1</sup> due to the substantial interaction between P-NMPy and MnSe. These findings provide strong validation for the fabricated MnSe/P-NMPy nanocomposite materials.

The RGO/MnSe was observed at 3422 cm<sup>-1</sup> indicates O–H bonding. C=C stretching vibration of RGO can be seen at 1628 cm<sup>-1</sup>. The C–O stretching vibrations of carboxyl and alkoxy groups are denoted by the peaks located at 1448 and 863 cm<sup>-1</sup>, respectively [26]. The FTIR spectrum shows peaks for RGO, MnSe, and P-NMPy, indicating that these components have successfully integrated into the structure of the nanocomposite. This accomplishment in synthesis shows that the ternary (RGO/MnSe@P-NMPy) polymer nanocomposite and binary (RGO/MnSe) nanocomposite have been effectively fabricated, with each component providing its unique spectrum characteristics. Consequently, the peaks observed in the FTIR spectrum serve as strong evidence of the successful synthesis and integration of RGO, MnSe, and P-NMPy into the polymer nanocomposite, confirming the desired composition and structure of the material.

The XRD pattern displayed in Fig. 1(c) depicts the crystal structures of the material. The prominent peak in the XRD image of pure MnSe is displayed in the figure, which corresponds to the (111), (210), (200), (220), (023), (321), (400), and (420) reflection peak, at  $2\theta = 19.01^{\circ}$ ,  $23.58^{\circ}$ ,  $29.77^{\circ}$ ,  $31.39^{\circ}$ ,  $41.46^{\circ}$ ,  $43.68^{\circ}$ ,  $45.44^{\circ}$  and  $51.74^{\circ}$ . Crystallographic planes depicts an RS type MnSe crystal structure (JCPDS-270311) [27]. The MnSe crystalline size was calculated to be

19 nm. The P-NMPy/MnSe polymer nanocomposite has five peaks, which are defined by the planes (111), (200), (310), (311), and (321) at  $2\theta = 23.66^{\circ}$ ,  $29.73^{\circ}$ ,  $43.73^{\circ}$ ,  $45.42^{\circ}$  and  $51.89^{\circ}$ . The average size of the P-NMPy/MnSe crystallite is 16 nm. The RGO/MnSe nanocomposite was estimated to be  $23.85^{\circ}$ ,  $30.08^{\circ}$ ,  $31.69^{\circ}$ ,  $41.67^{\circ}$ ,  $43.88^{\circ}$ ,  $45.65^{\circ}$ ,  $52.03^{\circ}$  and  $55.88^{\circ}$  are attributed to (111), (200), (211), (220), (221), (321), (310) and (311) illustrates the crystaline seen in the figure. The RGO/MnSe nanohybrid was determined to be 12 nm. In the equivalent lattice plane of (111), (210), (200), (222), (320), (321), and (331), the RGO/MnSe@P-NMPy polymer nanocomposite displays peaks at  $2\theta = 20.19^{\circ}$ ,  $23.46^{\circ}$ ,  $29.73^{\circ}$ ,  $41.36^{\circ}$ ,  $43.63^{\circ}$ ,  $45.28^{\circ}$ , and  $51.71^{\circ}$ . In the RGO/MnSe@P-NMPy nanohybrid material, the inclusion of RGO improved the MnSe crystal structure and decreased the peaks of selenium impurities. The RMP nanocomposite was discovered to have an average crystalline size of 10 nm. The active peak indicates the excellent crystalline clarity of MnSe. The connection between RGO, MnSe and P-NMPy polymer matrix is further confirmed by the variation in diffraction intensity.

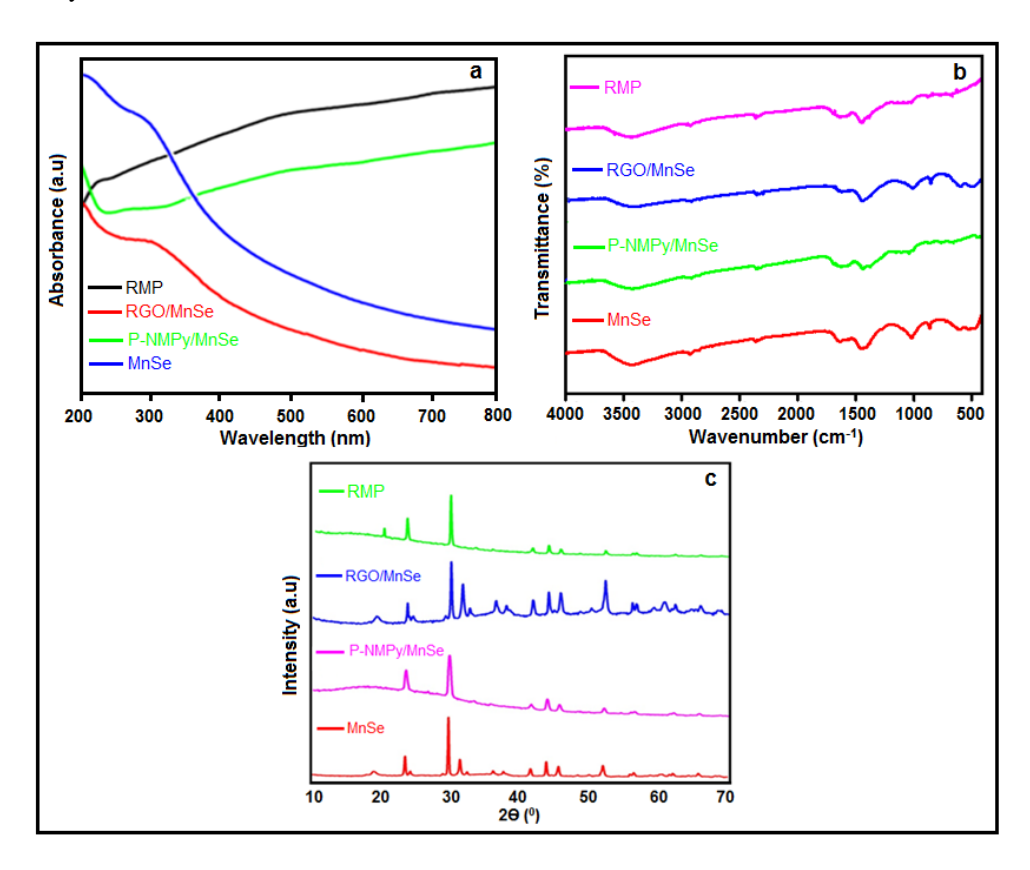


FIG. 1. a) UV-Visible spectra; b) FT-IR spectra and c) XRD patterns of MnSe, P-NMPy/MnSe, RGO/MnSe and RGO/MnSe@P-NMPy polymer nanocomposite

#### 3.2. Morphological study

FESEM depicts of MnSe, RGO/MnSe, P-NMPy/MnSe and RMP polymer nanohybride are displayed in Fig. 2. The result shows pure MnSe has a structure resembling a crystal. The P-NMPy/MnSe polymer nanocomposite showed sphere-like structure. It suggests that MnSe nanoparticles are evenly distributed across the P-NMPy's crumpled surface. The infected RGO in the RGO/MnSe nanomaterial was found to prevent the MnSe nanoparticles from clumping together as demonstrated in the figure. The RGO/MnSe nanocomposite exhibits a multilayer structure including a small quantity of micro nanoplates. P-NMPy was dispersed unifor mly across the RGO and MnSe nanocomposite. The RMP polymer nanocomposite revealed excellent dispersion as well as random distribution of NPs in the host polymer matrix indicating the formation of closely-packed uniform network structure. These nanoparticles were successfully mixed and dispersed unifor mly. The elemental mapping of selected area in RMP polymer nanocomposite was done by FESEM equipped with energy dispersive X-ray spectroscopy (EDX) mapping to verify the distribution of the elements (C, O, N, Mn and Se) and the obtained results (Fig. 3(a)) reveal good distribution of elements throughout the material. The synthesized RGO/MnSe@P-NMPy polymer nanocomposite is found to have a maximum atomic percentage of C and a minimum value of Se, Mn, O, and N, which confirmed the formation of the RGO/MnSe@P-NMPy polymer nanocomposite. Table 1 displays the atomic composition of the RGO/MnSe@P-NMPy polymer nanocomposite.

The microstructure of RMP nanohybrid was studied by TEM shows in Fig. 4 (a and b). Polymer was indicated by the black spot of the RGO layer. The nanoplates shape and uniformity remain disturbed by the incorporation of P-NMPy

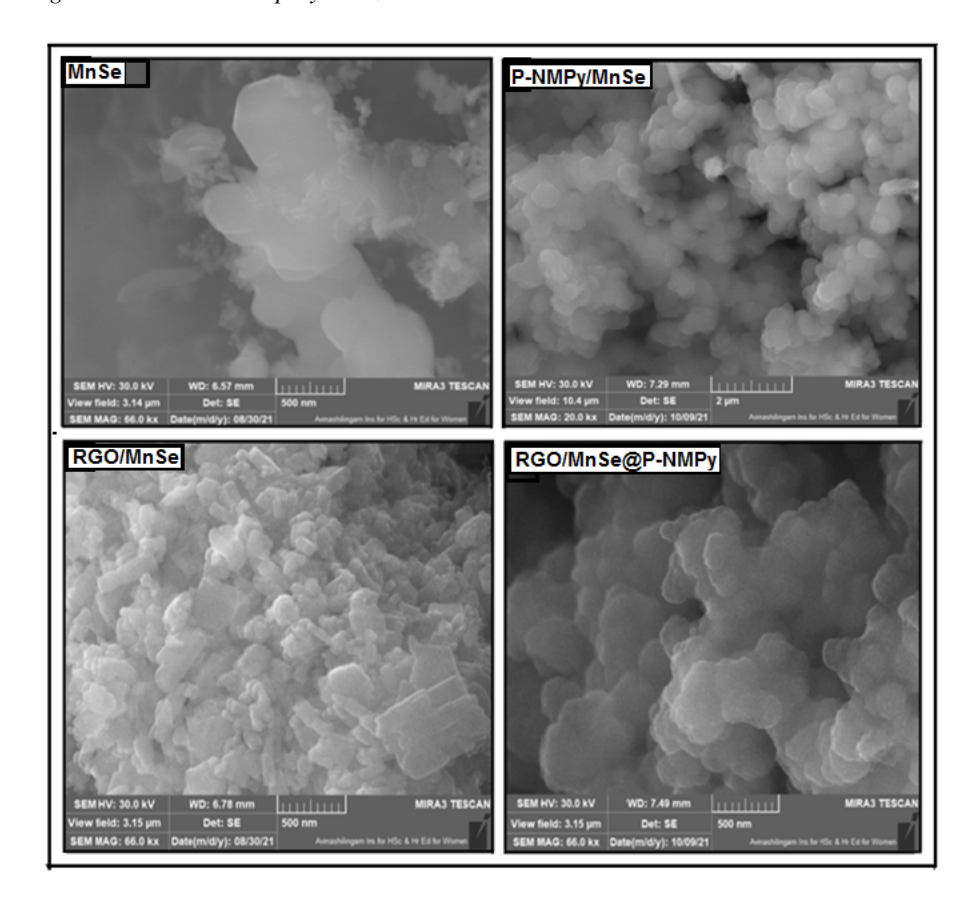


FIG. 2. FESEM images of MnSe, P-NMPy/MnSe, RGO/MnSe and RGO/MnSe@P-NMPy polymer nanocomposite

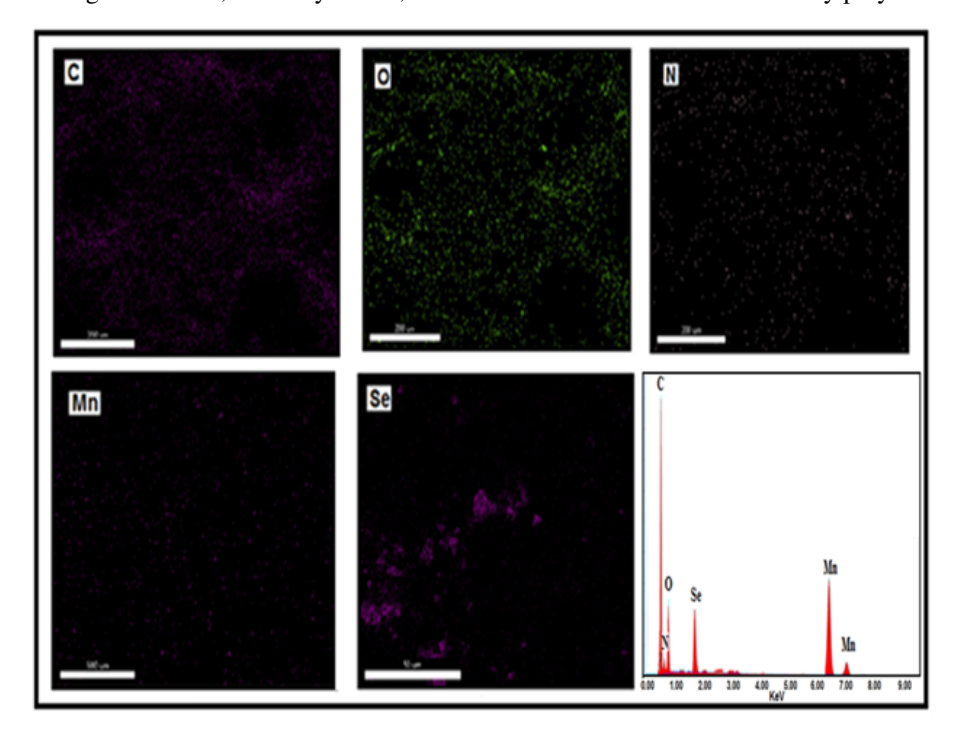


FIG. 3. Elemental mappings C, O, N, Mn and Se of RGO/MnSe@P-NMPy polymer nanocomposite

Sample	Element	Atomic %
RGO/MnSe@Poly-N-methyl pyrrole nanocomposite	С	69.12
	О	21.33
	N	2.16
	Mn	3.93
	Se	3.46

TABLE 1. Atomic composition of RGO/MnSe@P-NMPy polymer nanocomposite

in the RGO/MnSe matrix and its uneven spherical form. The TEM images clearly show that these nanoplates (Fig. 2) got well-dispersed over the thin graphene sheet, as was mentioned in the FESEM section. These findings are consistent with the elemental mapping investigations that were subjected to EDX analyses. (Fig. 3). Since P-NMPy was integrated into the RGO/MnSe matrix; the SAED pattern illustrates the transition from single-crystalline to polycrystalline nature.

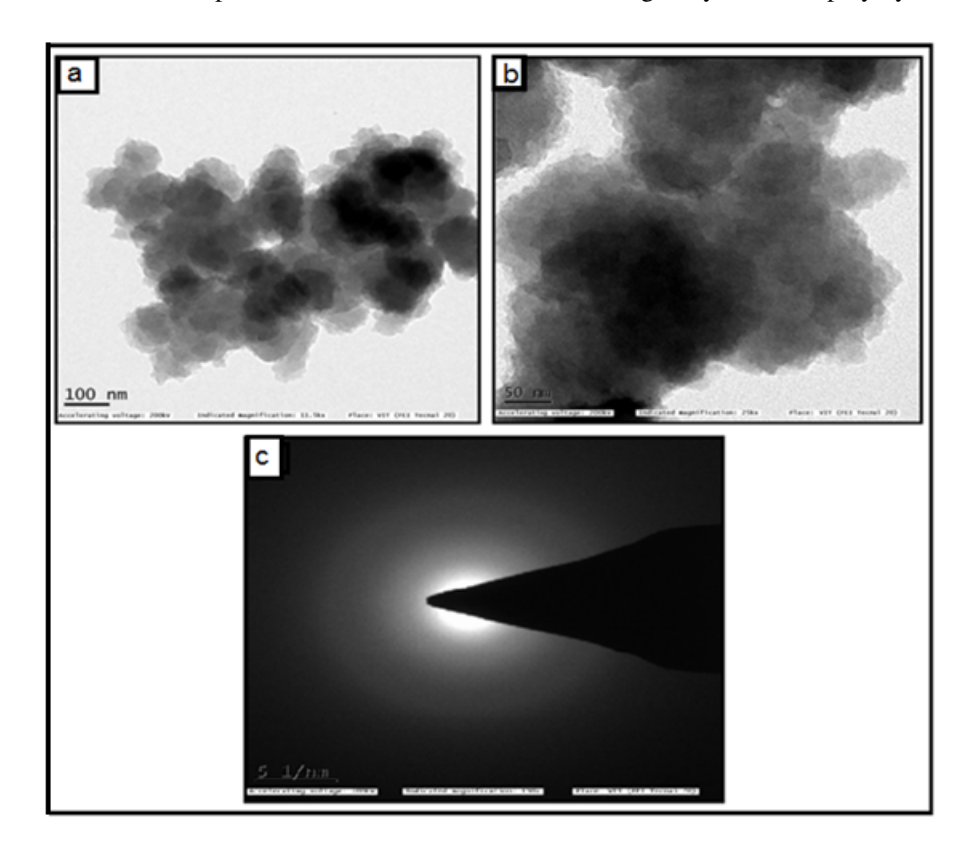


FIG. 4. TEM images of (a&b) RGO/MnSe@P-NMPy polymer nanocomposite and c) SAED pattern

## 3.3. Electrochemical measurements

3.3.1. Cyclic voltammetry activity of the modified polymer nanocomposite electrode. Cyclic voltammograms were used to examine the electrochemical behavior of MnSe, P-NMPy/MnSe, RGO/MnSe and RMP polymer nanocomposite. Platinum wire electrodes serve as a counter electrode, and the reference electrode is made of Ag/AgCl electrodes. The glassy carbon electrode (GCE) served as the working electrode for this experiment, it possesses an area of cross section is 0.0314 cm². Peak separation increases as scan rate increases, indicating the quasi-reversibility of the process of electron transfer. The peaks are acquired during different scan speeds of 30, 50, 100, 150 and 200 mVs<sup>-1</sup>. As illustrated in Fig. 5, modified electrodes were created in 0.5 M KOH. The potential range displayed by the MnSe nanoparticle is -1.2 to 1.2 V. The chemical nature of the peaks on the cyclic voltammograms measured in KOH solutions, often exhibit oxidation and reduction peaks. The potential range of 0.54 to 0.80 V, 0.08 to -0.18 and 0.63 to -0.91 V shows three reduction peaks, whereas the conspicuous peak of the oxidation peak is found at 0.85 to 1.10 V. The rate at which the electron transfer occurs between the working electrode and the solution redox species. This suggests that the electro chemical process is highly reversible. For the P-NMPy/MnSe polymer nanocomposites, an appropriate range of -1.0 to 1.2 V was observed.

The figure shows one anodic peak at -0.80 to 1.05 V and one cathodic peak with a potential range of 1.11 to 0.38 V. It revealed that in cathodic scan modes, RGO/MnSe nanocomposite display two separate peaks, while in anodic scan modes, there is only one peak. The range from -0.8 to 1.0 V represents the potential window. The range of the anodic peak potential is 0.68 to 0.93 V. There are two cathodic peak potential ranges: 0.0092 to -0.33 V and -0.41 to 0.65 V. The potential range of RMP polymer nanocomposite was found between -1.0 and 1.2 V. One oxidation peak can be observed in the anodic scan between 1.101 and 0.413 V and in the anodic scan between -0.82 and -1.0 V potential range.

Electrochemically active surface area (ECSA) of catalysts must be calculated in order to compare their electrocatalytic performance. By measuring the charge collected oxidation area, the ECSA for various catalysts was computed using the cyclic voltammograms (Fig. 5). Using the double layer capacitance (DLC) electrochemical measurement method is one frequently used method to determine the surface area. Therefore, a differential capacitance measurement (DCM) with a limited potential range and variable scan rates is being used. If this test is done in a range where there is no Faradic response, the resulting differential capacitance equals the double layer capacitance (CDL) [28]. The electrochemical active surface area (ECSA) can be computed using this capacitance by using the formula

$$ECSA = C_{dL}/C_{S}.$$
 (1)

The ECSA cannot be calculated without the specific capacitance (CS). The ECSA values for MnSe, P-NMPy/MnSe, RGO/MnSe and RGO/MnSe@P-NMPy polymer nanocomposite were calculated as follows: 69.9, 84.5, 129.2 and 183.7 m²/g, respectively. The value is the optimal flat surface capacitance of the catalyst. Electro-catalysts of methanol require multiactive centers to catalyze both oxygen reduction reaction (ORR) and oxygen evolution reaction(OER). This result clearly indicates that RGO/MnSe@P-NMPy polymer nanocomposite has more active sites than other electrocatalysts [26, 29]. The RMP polymer nanocomposite has a substantially higher ECSA value than the other MnSe, P-NMPy/MnSe and RGO/MnSe values, indicating a higher number of active sites.

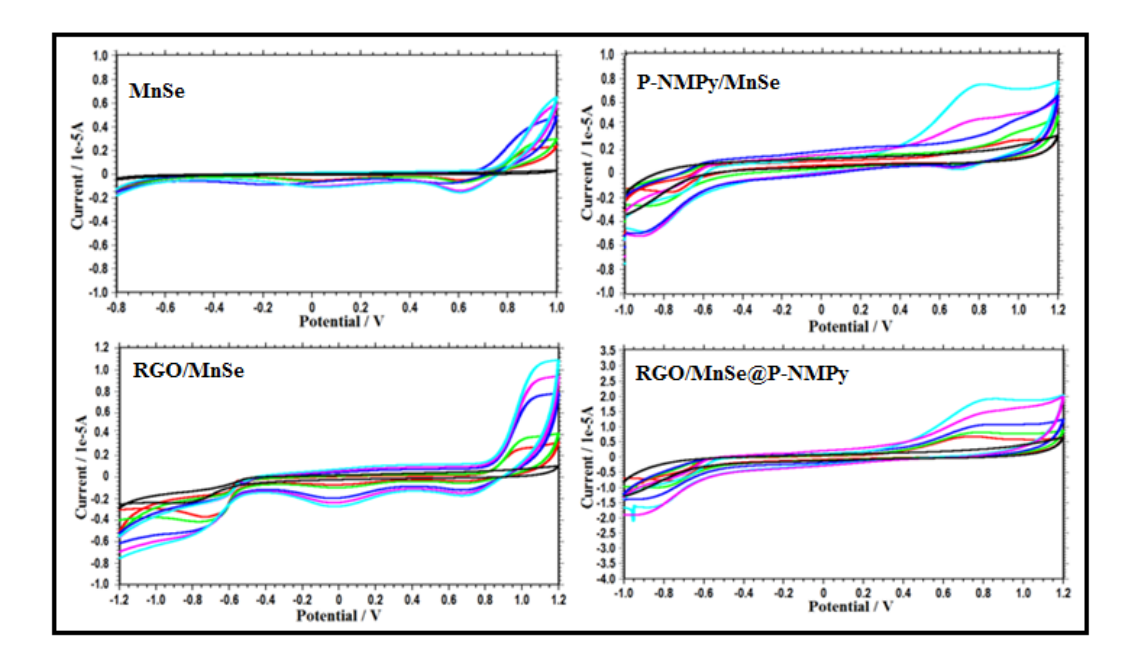


FIG. 5. Cyclic voltammetric behavior of MnSe, P-NMPy/MnSe, RGO/MnSe and RGO/MnSe@P-NMPy polymer nanocomposite in 0.5 M KOH at different scan rate (30, 50, 100, 150 and 200 mVs<sup>-1</sup>)

3.3.2. Electrochemical impedance measurements. Fig. 6 illustrates the charge transfer resistance of the as-prepared electrodes in a 0.5 M KOH solution using electrochemical impedance spectroscopy (EIS) curves. Similar semi-circular arcs were seen in the high frequency area of all EIS graphs, and the radius of these arcs indicates the electrode resistance's reaction to charge transfer. The electrochemical series resistance (ESR) of the symmetric cells is represented by the x-axis intercept of the half circle seen in the high-frequency region. The charge transfer resistance ( $R_{ct}$ ) at the electrode and electrolyte interface was identified as the cause of the arc seen in the high-medium frequency region. When compared to MnSe, P-NMPy/MnSe and RGO/MnSe, the resistance ( $R_s$ ) values of the RMP nanohybrid electrodes were lower, suggesting greater conductivity and better charge transfer. Because the impedance arc width of the RMP polymer nanocomposite was significantly smaller than that of the other materials, the EIS diagram showed the lowest electrical transfer resistance. The outcomes demonstrated that RGO/MnSe@P-NMPy polymer nanocomposite was advantageous to MOR.

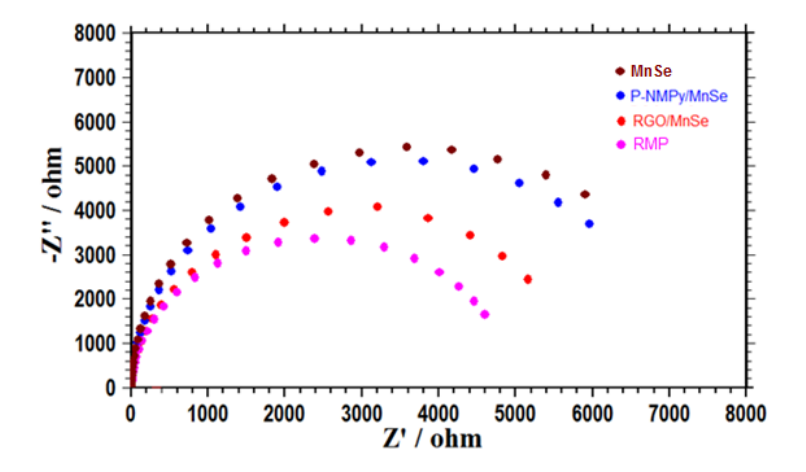


FIG. 6. EIS spectra of RGO, P-NMPy/MnSe, RGO/MnSe and RGO/MnSe@P-NMPy polymer nanocomposite

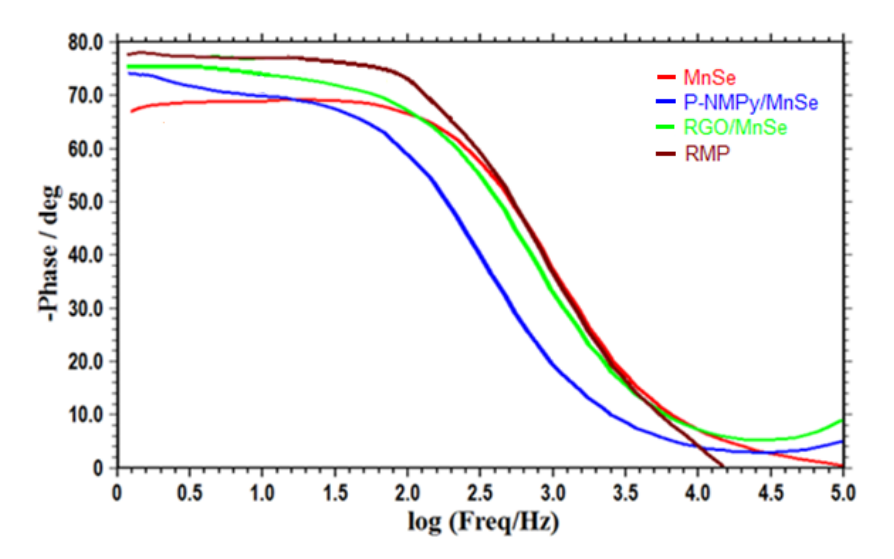


Fig.~7.~Bode~plot~of~phase~angle/~degree~versues~log(freq/Hz)~of~MnSe,~P-NMPy/MnSe,~RGO/MnSe~and~RGO/MnSe@P-NMPy~polymer~nanocomposite

3.3.3. Pseudo capacitive behavior. The Bode plot illustrates the Bode phase change with applied frequency. The phase angle  $\theta$  can range from 90° for a perfect capacitor (n=1), but it can be 0° for a perfect resistor (n=0) [30]. The Bode plot (-phase angle (degree) vs.  $\log f$  (Hz) is shown in Fig. 7. The value of n is obtained by plotting the frequency against the |Z| plot. The phase angle of 78° in the instance of RGO/MnSe@P-NMPy suggests that the material is pseudo capacitive. These findings imply that the behaviour of the RGO/MnSe@P-NMPy nanocomposite-coated electrode shifts from that of a pure resistor at high frequencies to that of pseudo capacitors at low frequencies. Bode phase angle of MnSe, P-NMPy/MnSe, RGO/MnSe and RGO/MnS@PMPyis found to be 67°, 73°, 76° and 78° respectively. It implies to a pseudo capacitor's characteristics. Bode phase angle values of MnSe, P-NMPy/MnSe, RGO/MnSe and RGO/MnSe@P-NMPy nanocomposite are presented in Table 2.

 $TABLE\ 2.\ Bode\ phase\ angle\ for\ MnSe,\ P-NMPy/MnSe,\ RGO/MnSe\ and\ RGO/MnSe@P-NMPy\ polymer\ nanocomposite$ 

Sl. No	Samples	<b>Bode phase angle</b> °
1.	MnSe nanoparticles	67
2.	P-NMPy/MnSe polymer nanocomposite	73
3.	RGO/MnSe polymer nanocomposite	76
4.	RGO/MnSe@P-NMPy polymer nanocomposite	78

### 3.4. Electrochemical application

3.4.1. Methanol oxidation pathway. As equations (2) and (3) make evident, an essential component of the reaction process in the oxidation of methanol is the supporting electrolyte. The complete oxidation of methanol in both acid and base media is a 6 electron oxidation that releases  $CO_2$ , as indicated by equations (2) for methanol oxidation in acidic medium and (3) for basic medium:

$$CH_3OH + H_2O \rightarrow CO_2 + 6H^+ + 6e^-,$$
 (2)

$$CH_3OH + 6OH^- \rightarrow CO_2 + 5H_2O + 6e^-.$$
 (3)

The aforementioned equations clearly show that the pH of the supporting electrolyte is critical during methanol oxidation given the roles that protons and hydroxide ions play in the overall reaction. In each step, several intermediate organic molecules are transported along with six electrons. Throughout this process, CO is the main poisoning species, whereas formate and  $CO_2$  (as carbonate) are the main dissolved products of the reaction. Studies in the literature indicate that because cations in solution have been demonstrated to affect reactions, Mn-based catalyst is appropriate for MOR reactions in alkaline media.

3.4.2. Oxidation of methanol using at various pH medium. As illustrated in Fig. 8, the CV was carried out using RMP polymer nanocomposite coated GCE in 1.0 M CH<sub>3</sub>OH, scanning at 100 mVs<sup>-1</sup> in the potential range of -1.0 to 1.2 V. The anodic current densities of RMP polymer nanocomposite varied significantly with different pH values; 63 mA/cm<sup>2</sup> at pH 1.0, 65 mA/cm<sup>2</sup> at pH 4.0, 58 mA/cm<sup>2</sup> at pH 7.0, 96 mA/cm<sup>2</sup> at pH 9.0 and 61 mA/cm<sup>2</sup> at pH 13.0. These results showed that the RMP polymer nanocomposite (pH 9.0) demonstrates the best conceivable methanol electro-oxidation efficiency in an alkaline medium [30]. The outcome of MnSe nanoparticles, RGO and P-NMPy is responsible for the higher electrochemical performance of ternary compound. Notably, Fig. 8 shows that pH 9.0 exhibits the highest current density and anodic oxidation potential, confirming its superior catalytic activity for methanol oxidation reactions (MOR) [32].

The electro-catalyst of RGO/MnSe@P-NMPy polymer nanocomposite has higher oxidation peaks at 0.9 V (pH 9) [33]. At this potential, it was proposed that methanol oxidation appears as a moderate increase in current density. These results clearly show that Mn/Se participates directly in this electro-catalytic methanol oxidation process. In the region around  $\sim 0.9 \text{ V}$ , at which only Mn species exist at the electrode surface, a new anodic peak was usually observed with a larger peak current (96 mA/cm² at pH 9.0) than that of alkali electrolyte (25 mA/cm²) [34,35]. The height of this peak increases linearly with the methanol concentration in the solution, showing that it is related to a process involving methanol, in good agreement [36].

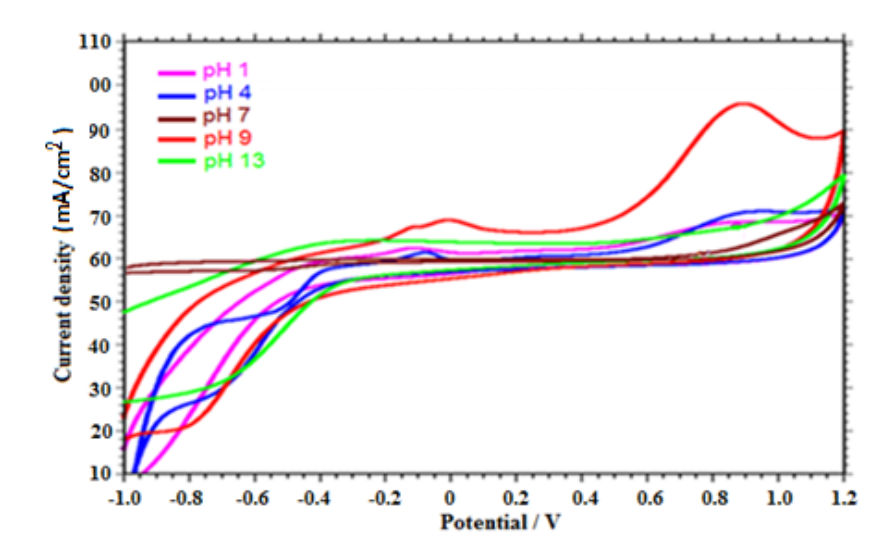


FIG. 8. Cyclic voltammogram of methanol using RGO/MnSe@P-NMPy polymer nanocomposite of pH 1.0, pH 4.0, pH7.0, pH 9.0 and pH 13.0

3.4.3. Chronoamperometry studies. Chronoamperometric measurements are a valuable technique for assessing catalyst stability. Modified anodes were subjected to extended tests at lower voltages against an Ag/AgCl electrode in 1.0 M CH<sub>3</sub>OH and 0.5 M KOH. Fig. 9 displays chronoamperometry results for each catalyst used in methanol oxidation reactions. These curves illustrate how the initial adsorption of poisoning intermediates causes a rapid decline in current density, which then stabilizes over time. Notably, due to its higher ECSA (electrochemical surface area) and reduced CO poisoning effects, RGO/MnSe@P-NMPy nanohybrid exhibits a slower initial drop in current density and ultimately achieves a higher final current density compared to other materials [37, 38]. The findings indicate that RGO/MnSe@P-NMPy

polymer nanocomposite demonstrates superior stability and catalytic efficiency for methanol oxidation, as evidenced by the highest sustained current density observed in Fig. 9 [39]. The comparison of current density values from the figures reveals distinct performances: MnSe (13.00 – 0.38 mA/cm²), P-NMPy/MnSe (15.27 – 0.58 mA/cm²), RGO/MnSe (18.39 – 0.72 mA/cm²), and RGO/MnSe@P-NMPy (27.71 – 0.97 mA/cm²). This analysis underscores the synergistic impact of RGO/MnSe@P-NMPy polymer nanocomposite, which demonstrates remarkable catalytic activity as our proposed catalyst. The synergistic effect observed in the hybridization of multiple species enhances catalytic performance by leveraging complementary strengths and compensating for the limitations of individual active sites. This approach is pivotal in advancing catalyst design for efficient electrochemical processes.

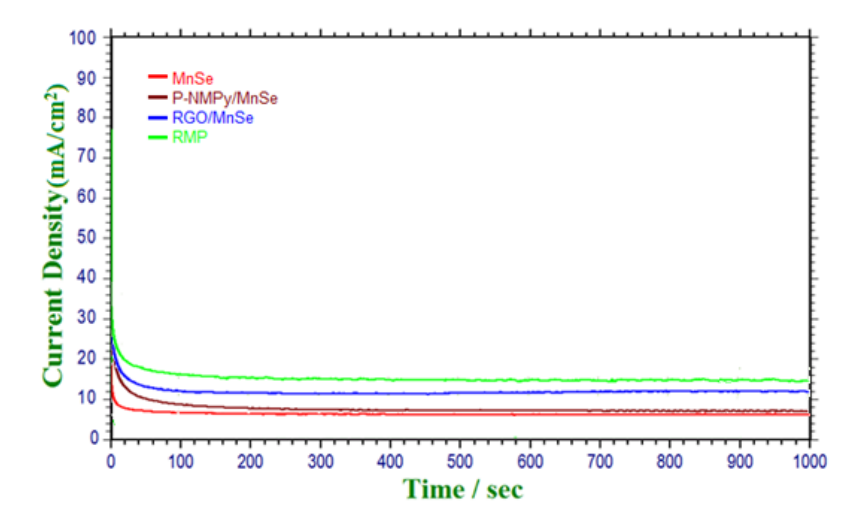


FIG. 9. Chronoamperometric curves of MnSe, P-NMPy/MnSe, RGO/MnSe and RGO/MnSe@P-NMPy polymer nanocomposite

## 4. Conclusion

MnSe nanoparticles supported on P-NMPy and RGO surfaces were synthesized using a novel and straightforward method. These were successfully utilized to modify RMP polymer nanocomposites, creating active electrodes for methanol oxidation reactions (MOR). One significant characteristic of the polymer nanocomposite is its ability to adopt a spherical shape, which likely contributes to enhanced MOR electrocatalytic activity. This approach suggests potential for multifunctional electrode applications in electrocatalysis. Characterization analyses confirm that MnSe nanoparticles are evenly dispersed within the RGO/P-NMPy matrix. The electrocatalytic performance of these catalysts in the oxidation of methanol (CH<sub>3</sub>OH) in basic media was extensively studied. The RGO/MnSe@P-NMPy polymer nanocomposite exhibited a notable current density of 96 mA/cm<sup>2</sup> when exposed to methanol. The synergistic interaction among MnSe nanoparticles, P-NMPy and RGO (RMP) polymer nanocomposite significantly enhances their electrochemical and electrocatalytic capabilities. The RMP polymer nanocomposite electro-catalyst demonstrated an ECSA value of 183.7 m<sup>2</sup>/g, indicating a high density of active sites crucial for MOR. During chronoamperometric measurements over extended periods (1000's), the RMP polymer nanocomposite modified electrode showed a higher initial current density (27.71 mA/cm<sup>2</sup>) and a slower decline, ultimately achieving a stable state. This stability and high current density during electrochemical MOR highlight the superior performance of the RGO/MnSe@P-NMPy catalyst. These attributes underscore the potential of this catalyst for industrial-scale electrolysis, validated by its high electrocatalytic activity and robust electrochemical stability in methanol oxidation applications.

## References

- [1] Compton O.C., Jain B., Dikin D.A., Abouimrane A., Amine K., Nguyen S.T. Chemically active reduced graphene oxide with tunable C/O ratios. *ACS Nano*, 2011, 5 (6), P. 4380–4391.
- [2] Ennaoui A., Fiechter S., Jaegermann W., Tributsch H. Photo electrochemistry of highly quantum efficient single-crystalline n-FeS<sub>2</sub> (pyrite). *J. Electrochem. Soc.*, 1986, **133**, P. 97–106.
- [3] Kwon S.G., Hyeon T. Collodial Chemical Synthesis and Formation Kinetics of Uniformly Sized Nanocrystals of metals, Oxides and Chalcogenides. *Acc. Chem. Res.*, 2008, **41**, P. 1696–1709.
- [4] Johari P., Shenoy V.B. Tuning the electronic properties of semiconducting transition metal dichalcogenides by applying mechanical strains. ACS Nano, 2012, 6, P. 5449–5456.
- [5] Wang D.S., Zheng W., Hao C.H., Peng Q., Li Y.D. A Synthetic Method for Transition-Metal Chalcogenide Nanoccrystals. Chem. Eur. J., 2009, 15, P. 1870–1875.
- [6] Santra P.K., Kamat P.V. Mn-Doped Quantum Dot Sensitized Solar Cells: A Strategy to Boost efficiency over 5 %. J. Am. Chem. Soc., 2012, 134, P. 2508–2511.

- [7] Wang L., Chen L., Luo T., Bao K., Qian Y. A facile method to the cube-like MnSe<sub>2</sub> micro crystallines via a hydrothermal process. *Solid State Commun.*, 2006, **138**, P. 72–75.
- [8] Sobhani A., Salavati-Niasari M. Morphological control of MnSe<sub>2</sub>/Se nanocomposites by amount of hydrazine through a hydrothermal process. Mater. Res. Bull., 2013, 48, P. 3204–3210.
- [9] Zheng L., Li J., Zhou B., Liu H., Bu Z., Chen B., Ang R., Li W. Thermoelectric properties of p-type MnSe. J. Alloy Comp., 2019, 789, P. 953–959.
- [10] She Z.W., Kibsgaard J., Dickens C.F., Chorkendoree I., Norskov J.K., Jaramillo T.F. Combine in theory and experiment in electrocatalysis: Insight into materials design. *Science*, 2017, 355.
- [11] Wang J., Liao T.L., Wei Z., Sun J., Guo J., Sun Z. Heteroatom-doping of non-noble metal-based catalysts for electrocatalytic for hydrogen evolution: an electronic structure tuning strategy. *Small Methods*, 2021, **5**.
- [12] Suh J., Tan T.L., Zhao W., Park J., Lin D.Y., Park T.E., Kim J., Jin C., Saigal N., Ghosh S., Wong Z., Chen Y., Wang F., Walukiewicz W., Eda G., Wu J. Reconfiguring crystal and electronic structures of MoS<sub>2</sub> by substitutional doping. *Nat. Commun.*, 2018, **9**, P. 199.
- [13] Santhosh S., Teller H., Schechter A., Kalarikkal N. Effect of Mndoped NI-Co mixed oxide catalysts on urea oxidation. Chem. Catchem., 2022, 14.
- [14] Li W., Liang C., Qiu J., Zhou W., Han H., Wei Z. Carbon nanotubes as support for cathode catalyst of a direct methanol fuel cell. *Carbon*, 2002, 40, P. 787–790.
- [15] Zhang L., Zhang D., Ren Z. Mesoporous NiCo<sub>2</sub>O<sub>4</sub> micro/nanospheres with Hierarchicals structures for Supercapacitors and Methanol Electro-oxidation. Chem. Electro Chem., 2017, 4, P. 441–449.
- [16] Wu J.B., Li Z.G., Huang X.H., Lin Y.J. Porous Co<sub>3</sub>O<sub>4</sub>/NiO core/shell nanowire array with enhanced catalytic activity for methanol electro-oxidation. *Power Sources*, 2013, 224, P. 1–5.
- [17] Li Z., Li M., Han M., Zeng J., Li Y., Guo Y., Liao S.J. Preparation And Characterization Of Carbon-Supported PTOs electrocatalysts via polyol reduction method for methanol oxidation reaction. *Power Sources*, 2014, 268, P. 824–830.
- [18] Zhang W., Pan Z., Yang F.K., Zhao B. A facile in situ approach to polypyrrole functionalization through bioinspired catechol. Adv. Funct. Mater, 2015, 25, P. 1588–1597.
- [19] Abaci U., Guney H.Y., Kadiroglu U. Morphological and electrochemical properties of PPy, PAni bilayer films and enhanced stability of their electrochromic devices (PPy/Pani-PEDOT, Pani/PPy-PEDOT). *Electrochim. Acta*, 2013, **96**, P. 214–224.
- [20] Vellaichamy B., Periakaruppan P. Silver nanoparticle-embedded RGO-nano sponge for superior catalytic activity towards 4-nitrophenol reduction. *RSC Advances*, 2016, **6**, P. 88837–88845.
- [21] Wu X., Zhou J., Xing W., Wang G., Cui H., Zhuo S. High-rate capacitive performance of graphene aerogel with a super high C/O molar ratio. *J. of Materials Chemistry*, 2012, **22**, P. 23186–23193.
- [22] Vellaichamy B., Prakash P., Thomas J. Synthesis of AuNPs@RGO nanosheets for sustainable catalysis toward nitrophenols reduction. *Ultrasonics Sonochemistry*, 2018, 48, P. 362–369.
- [23] Onari S., Arai T. Infra-red lattice vibrations and dielectric dispersion in antiferro magnetic semiconductor MnSe<sub>2</sub>. J. Phys. Soc. Jpn., 1979, 46, P. 184–188.
- [24] Gemeiner P., Kulocek J., Mikula M., Hatala M., Sovre L., Hlavata L., Micusl M., Omastova M. Polypyrrole coated multi-walled carbon nanotubes for the simple preparation of counter electrodes in dye-sensitized solar cells. Synth. Met., 2015, 210, P. 323–331.
- [25] Xu C., Sun J., Gao L. Synthesis of novel hierarchical graphene/polypyrrole nanosheet composites and their superior electrochemical performance. *J. of Materials Chemistry*, 2011, **21**, P. 11253–11258.
- [26] Zhu C., Guo S., Fang Y., Dong S. Reducing sugar: New functional molecules for the green synthesis of graphene nanosheets. ACS NAno, 2010, 4, P. 2429–2437.
- [27] Murrary R.M., Forbes B.C., Heyding R.D. The Copper-Selenium System at Temperatures to 850 K and Pressures To 50 Kbar. J. of Chemistry, 1975, 53, P. 4059–4061.
- [28] Meher S.K., Rao G.R., Jia Y. Coatings in glewalled carbon nanotube with SnO<sub>2</sub> and its electrochemical properties. *Power Technol.*, 2012, 224, P. 306–310
- [29] Bing Zhang, Shaofeng Lin, Jingjing Zhang, Xiaopeng Li, Xiaodong. Sun Facile Synthesis of Sandwich-Like rGO/CuS/Polypyrrole Nano architectures for Ecient. Electromagnetic Absorption Materials, 2020, 13, 446.
- [30] Bajpai A.K., Bhatt R.K., Kaatare R. Atomic force microscopy enabled roughness analysis of nanostructured poly (diaminonaphthalene)dopedpoly(vinyl alcohol) conducting polymer thin flims. *Micron*, 2016, **96**, P. 12–17.
- [31] Fajin J.L., Cordeiro M.N.D. Insights into the mechanism of methanol steam reforming for hydrogen production over Ni-Cu-Based Catalysts'. American Chemical Society of Catalyst, 2021, 12, P. 512–526.
- [32] Chang R., Zheng L., Wang C., Yang D., Zhang G., Sun S. Synthesis of hierarchic al platinium-palladium-copper nanodendrites for efficient methanol oxidation. *Appl. Catal. B: Environ.*, 2017, **211**, P. 205–211.
- [33] Kavitha M., Muthuchudarkodi R.R., Shakina J. NiSe integrated with Polymerized Reduced Carbon Sheet: As an effective electro-catalyst formethanol oxidation. Int. J. Hydrogen Energy, 2024, 51, P. 1050–1059.
- [34] Asgari M., Maragheh M.G., Davarkhah R., Lohrasbi E. Methanol Electrooxidation on the Nickel Oxide Nanoparticles/Multi-Walled Carbon Nanotubes Modified Glassy Carbon Electrode Prepared Using Pulsed Electrodeposition. J. Electochem. Soc., 2011, 158, K225–K229.
- [35] Seghiour A., Chevalet J., Barhoum A., Lantelme F. Electrochemical oxidation of nickel in alkaline solutions: a voltammetric study and modelling. *J. Electroanal. Chem.*, 1998, **442**, P. 113–123.
- [36] Pieta I.S., Rathi A., Pieta P., Nowakowski R., Hołdynski M., Pisarek M., Kaminska A., Gawande M.B., Zboril R. Electrocatalytic methanol oxidation over Cu,Ni and bimetallic Cu–Ni nanoparticles supported on graphitic carbon nitride. *Applied Catalysis B: Environmental*, 2019, 244, P. 272–283.
- [37] Gracita M., Tomboc, Hern Kim. Utilization of the superiorproperties of highly mesoporous PVP modified NiCo<sub>2</sub>O<sub>4</sub> with accessible 3D nanostructure and flower-like morphology towards electrochemical methanol oxidation reaction. *J. of Energy Chemistry*, 2018, **29**, P. 136–146.
- [38] Daryoush Afzali, Fariba Fathirad, Zahra Afzali, Mehdi Esmaeili Bidhendi. Design of PdxIr/g-C<sub>3</sub>N<sub>4</sub> modified FTO to facilitate electricity generation and hydrogen evolution in alkaline media. *Int. J. of Hydrogen Energy*, 2020, 45, P. 22965–22972.
- [39] Meenakshi Choudhary, Samarjeet Siwal, Debkumar Nandi, Kaushik Mallick. Catalytic performance of thein situ synthesized palladium– polymer nanocomposite. New J. Chem., 2016, 40, P. 2296–2303.

Information about the authors:

*Kavitha Murugan* – PG and Research Department of Chemistry, V.O. Chidambaram College, Thoothukudi-628008, Tamilnadu. Affiliated to Manonmaniam Sundaranar University, Abishekapatti, Tirunelveli-627012, Tamilnadu, India; ORCID 0009-0000-7962-8666; kavithakrithiv35@gmail.com

*Kalaiarasi Senthurpandi* – PG and Research Department of Chemistry, A.P.C Mahalaxmi College for Women, Thoothukudi-628002, Tamilnadu, Affiliated to Manonmaniam Sundaranar University, Abishekapatti, Tirunelveli-627012, Tamilnadu, India; ORCID 0000-0001-6855-8375; kalaiarasi@apcmcollege.ac.in

*Vedhi Chinnapaiyan* – PG and Research Department of Chemistry, V.O. Chidambaram College, Thoothukudi-628008, Tamilnadu. Affiliated to Manonmaniam Sundaranar University, Abishekapatti, Tirunelveli-627012, Tamilnadu, India; ORCID 0000-0002-3446-0641; cvedhi23@gmail.com

*Muthuchudarkodi Rajaram* – PG and Research Department of Chemistry, V.O. Chidambaram College, Thoothukudi628008, Tamilnadu. Affiliated to Manonmaniam Sundaranar University, Abishekapatti, Tirunelveli-627012, Tamilnadu, India; ORCID 0000-0002-2769-8045; muthu.rajaram@gmail.com

Conflict of interest: The authors declare that they have no known competing financial interests or personal relationships that could have appeared to influence the work reported in this paper.